An original semi-discrete approach to assess gas conductivity of concrete structures

Mohamad Ezzedine El Dandachy, Matthieu Briffaut, Frédéric Dufour, Stefano Dal Pont

An original semi-discrete approach to assess gas conductivity of concrete structures

M. Ezzedine El Dandachy*,†, M. Briffaut, F. Dufour and S. Dal Pont

University Grenoble Alpes, 3SR, F-38000 Grenoble, France

For civil engineering structures with a tightness role, structural permeability is a key issue. In this context, this paper presents a new proposition of a numerical modelling of leakage rate through a cracked concrete structure undergoing mode I cracking. The mechanical state of the material, considered in the framework of continuum mechanics based on finite element modelling, is described by means of the stress-based nonlocal damage model which takes into account the stress state and provides realistic local mechanical fields. A semi-discrete method based on the strong discontinuity approach to estimate crack opening is then considered in the post-treatment phase. Using a Poiseuille's like relation, the coupling between the mechan-ical state of the material and its dry gas conductivity is performed.

For validation purposes, an original experimental campaign is conducted on a dry concrete disc loaded in a splitting setup. During the loading, gas conductivity and digital image correlation analysis are performed. The comparison with the 3D experimental mechanical global response highlights the performance of the mechanical model. The comparison between crack openings measured by digital image correlation and estimated by the strong discontinuity method shows a good agreement.

Finally, the results of the semi-discrete approach coupled with the gas conductivity compared with exper-imental data show a good estimation of the structural conductivity. Consequently, if the mechanical problem is well modelled at the global scale, then the proposed approach provides good estimation of gas conductivity.

KEY WORDS: continuum mechanics; semi-discrete approach; damage; gas conductivity; splitting test; mortar concrete

1. INTRODUCTION

During their service life, due to external loading (mechanical and/or thermal, environmental, etc.), concrete structures may undergo cracking in a diffuse manner (microcracking) and/or localized cracking (macrocracking). Those degradations may directly affect the durability of the structure. Structural permeability is even a service criterion for structures with a tightness role such as confinement vessels of nuclear power plant. Therefore, the estimation/prediction of the evolution of transfer properties in such a cracked structure based on numerical modelling is a key issue for structural durability analysis. However, estimation of the transfer property evolution of cracked structures is not possible before understanding the physics behind the means of experiments performed at the material scale. Three different regimes of radial permeability evolution are seen during a compression test applied on hollow concrete cylinders [1]. A first regime exhibiting a slight permeability increase due to the presence of microcracks spreads out in the material [2]. In this diffuse regime, coupling between permeability and microcracking modelled by a damage variable

*Correspondence to: M. Ezzedine El Dandachy, University Grenoble Alpes, 3SR, F-38000 Grenoble, France.
†E-mail: mohamad.ezzedineeldandachy@3sr-grenoble.fr; www.3sr-grenoble.fr

has been proposed when the material is in compression [3–5] and when the material is subjected to high temperatures [6]. A second regime is observed during which the permeability of the material increases rapidly due to the cracking coalescence which provides both new porosity and an increase of the connectivity. A third regime is observed when macrocracks are formed and permeability is governed at the structural level by Poiseuille's law (fluid conductivity of a space between parallel plates) and mainly depends on the crack opening. This regime is characterized by a slower rate of permeability increase with respect to the second regime. Many authors [7–12] have shown that Poiseuille's law overestimates a fluid flow in a real crack because secondary effects such as crack roughness, crack opening variation and tortuosity are not taken into account. A correction factor, generally denoted as ξ in the literature, is introduced in order to account for those geometrical parameters. As a first approximation, this factor can be supposed to be constant for a given concrete. For instance, load-induced cracks in high-performance concrete should be smoother than the tensile cracks in ordinary concrete (OC), and therefore the correction factor might be lower for OC [7]. However, a recent study on water permeability evolution of a localized crack in concrete under splitting test has recently proposed an empirical relation for the correction factor which depends on the crack opening [8, 9]. In this way, the wall effect provided by the crack roughness is relatively dependent on the crack opening.

Numerical models for structural behaviour, cracking assessment and transfer behaviour are needed for a good description of the material degradation and to estimate/predict the evolution of the gas permeability of the material. Many numerical models that aim to describe the mechanical response of concrete structures under mechanical loading exist in the literature. Among the existing models, some can explicitly describe the cracking in the mechanical model, as shown in extended finite element method (FEM) [13], generalized FEM [14], embedded FEM [15, 16] or lattice models [17, 18] for instance. The advantage of those models is that the location of the crack and the crack opening are directly quantified. Nevertheless, the modelling of the crack initiation and crack propagation accounting for the bulk dissipation (fracture process zone) are still open issues or numerically very demanding in 3D. Besides, another class of numerical models based on continuum damage mechanics is a good candidate for cracking estimation [19]. Herein, the microcracking process and the macrocracking failure are implicitly described and can be modelled by using regularization techniques to avoid mesh dependencies [20, 21]. Those models are able to predict the initiation and the propagation of the cracking and account for size effects. Furthermore, if needed, crack properties (path and opening) can be estimated in a post-processing phase with a good agreement compared with experimental results [22–25]. Consequently, continuous damage models are preferred in this contribution. In this work, the stress-based nonlocal (SBNL) regularization technique [20, 22] is used to provide a realistic damage field based on the Mazars criterion [19] to represent microcracking and macrocracking during failure. This technique provides sharp strain profiles upon complete failure which allows to deal with multiple close localized cracks without overlapping of their strain profiles [22].

To assess material permeability with damage models, a fully continuous approach has been proposed in order to relate the mechanical state of the material and its permeability to gas [26]. It consists of using a matching law between the Picandet's permeability relation [3] (Darcy's percolation through the interconnected pores) and the Poiseuille's permeability (percolation through macrocracks). Herein, the two permeabilities are directly related to damage. This law is straightforward and does not require a numerical crack opening assessment. The damage field directly provides, using the matching law, a permeability field that is used in a second step for a diffusion problem to assess the structural conductivity. The main concern with this approach is that empirical permeability-damage relations identified on specific experimental test (compression, splitting, etc.) are not always valid for any loading case and specimen geometry (see [3–5]). Besides, because the experimental damage is assessed from the structural response and is certainly not valid for extreme loading for which crack localization is obtained, a material law can no longer be derived. A second possibility to find a coupling by using damage models is to consider a semi-discrete approach, which is the approach proposed in this contribution. The main difference is that after solving the mechanical problem, additional numerical tools are used to locate the crack and quantify its opening. The semi-discrete approach together with the constitutive laws are detailed in Section 2.

Despite existing studies in the literature [1,3,7–12], there are still some needs for more knowledge on gas conductivity of cracked structures because there is no study on a single cracked concrete specimen for which the crack is fully assessed and the percolated fluid does not interact with the cement matrix. To this end and to validate the semi-discrete approach, an experimental campaign has been performed on mortar specimens subjected to splitting test; the gas permeability of the specimens is measured during the tests at different load levels. Crack opening displacements (CODs) are estimated by means of digital image correlation (DIC; Section 3). The validation of the proposed gas permeability-mechanical model against experimental results is performed on the leakage rate perpendicular to the disc for different load stages (Section 4).

2. SEMI-DISCRETE APPROACH

The semi-discrete approach consists of using a regularized damage model for the mechanical description. In principle, any model can be used as long as it provides a precise description of local fields. In this contribution, the SBNL damage model [20, 22] applied to the Mazars criterion [19] is chosen. The next step is to assess the crack path either by using for instance a topological search [23] or the global tracking algorithm [24]. Once the crack path is found, the COD can be computed along the discretized crack surface by using a strong discontinuity method in the post-processing phase [25]. In this framework, each damaged FE of the crack path is represented as an equivalent porous medium with effective gas transfer-mechanical properties. The representation is carried out by means of the element crack opening. The final step is to prescribe the modified Poiseuille's law along the crack path, taking into account the roughness, crack opening variation and tortuosity of the crack to estimate the leakage rate whilst imposing a pressure gradient in the crack surface.

2.1. Stress-based nonlocal damage model

The loss of stiffness associated to mechanical degradation of the material is characterized by a scalar damage variable D. This internal variable links the Cauchy stress tensor $\boldsymbol{\sigma}$ to the strain tensor $\boldsymbol{\varepsilon}$, following:

$$\boldsymbol{\sigma} = (1 - D)\mathbf{C} : \boldsymbol{\varepsilon} \tag{1}$$

where C is the fourth order tensor of elastic moduli. The variable D ranges from 0 for a virgin material to 1 for a completely damaged material. It is assumed that D depends on a state variable Y, which in turn depends on the strain tensor, $Y = Y(\boldsymbol{\varepsilon})$.

The nonlocal regularization method on the internal variable Y is used in order to maintain the objectivity of the results by averaging the state variable Y in the neighbourhood of each point [21]. This method of regularization replaces a local variable Y by its nonlocal counterpart $\tilde{Y}$ as:

$$\tilde{Y} = \frac{\int_{\mathrm{v}} \alpha(d) Y dV}{\int_{\mathrm{v}} \alpha(d) dV} \tag{2}$$

The weight function α depends on the distance d to the point under consideration. Generally, a Gaussian function is used:

$$\alpha(d) = \exp\left[-\left(\frac{2d}{l_{\mathrm{c0}}}\right)^2\right] \tag{3}$$

where l_{c0} is a model parameter of the nonlocal damage model called internal length and Y is the state variable that controls the damage $\left(D = D\left(\tilde{Y}\right)\right)$ according to the Mazars criterion [19]:

$$Y = \sqrt{\sum_i [\max(0, \varepsilon_i)]^2} \tag{4}$$

The damage evolution follows a law which distinguishes tensile damage D_t and compressive damage D_c:

$$D = \alpha_t{}^{\beta_s} D_t + \alpha_c{}^{\beta_s} D_c \tag{5}$$

where α_t and α_c are the weights computed from the strain tensor and β_s is a parameter accounting for shear behaviour generally equal to 1.06. The tensile damage D_t and compressive damage D_c are calculated as follows:

$$D_{t,c} = 1 - \frac{Y_{D0}\left(1 - A_{t,c}\right)}{\tilde{Y}} - \frac{A_{t,c}}{e^{\left[B_{t,c}\left(\tilde{Y} - Y_{D0}\right)\right]}} \tag{6}$$

where A_t, A_c, B_t and B_c are model parameters; Y_{D_0} is the strain at first crack in tension and is also called the damage threshold. The Mazars model is chosen for its capacity, with a minimum number of parameters to accurately capture cracking initiation and propagation. However, it does not account for permanent deformation and is thus rather brittle during unloading phases.

This regularization method allows the objectivity of the results. However, it fails to properly describe both the strain field and the damage profile at complete failure as well as cracking initiation close to boundaries [27]. In order to improve the description of the continuous fields, an evolution of nonlocal interactions should be introduced in computations. In the present contribution, the method proposed in Refs [20, 22] is used. This regularization method, called the SBNL, is characterized by a regularization that takes into account the stress state of the material. A modification of the Gaussian function is applied, and the interaction function becomes:

$$\alpha(d) = \exp\left[-\left(\frac{2d}{l_{c0} * \rho}\right)^2\right] \tag{7}$$

where ρ is a stress factor calculated for each integration point and depends on the principal stresses of the medium. With this regularization technique, the strain profile tends to be localized on one set of elements upon failure. In other words, the nonlocal interaction with the stress-based technique is reduced the more the closer to failure until the strain profile becomes narrow at complete failure. This feature permits to obtain two (or more) close localized cracks without overlapping of their correspondent strain profiles. More details can be found in Refs [20, 22].

This nonlocal damage model is used in this contribution to simulate the mechanical state. Once the mechanical state is obtained, the transfer properties have to be derived.

2.2. Coupling permeability with the mechanical state

2.2.1. Darcy's law. Assuming that the flow is laminar, Darcy's law [28] is used to determine the mean structural permeability (gas conductivity) of the concrete structure. For a unidirectional flow, the mean structural permeability k_m is determined as:

$$k_m = -\frac{\mu}{grad(P)} \frac{Q}{A} \tag{8}$$

where A (m^2) is the cross section of the specimen that is perpendicular to the flow direction, $grad(P)$ is the pressure gradient (Pa/m), μ is the dynamic viscosity of the fluid at 20 °C, and Q is the total volumetric flow rate through the sample (m^3/s).

2.2.2. The modified Poiseuille's law. In order to numerically find the total volumetric flow rate through a cracked concrete structure by using a FE computation, a permeability model has to be defined. The simplest model of an incompressible fluid flow through a crack is the parallel plate

model [29, 30] (Poiseuille's law). Poiseuille's permeability for concrete is identified by solving Navier–Stokes equation for two fracture walls modelled as two smooth parallel plates, distant by a distance $[u]$ [31]. However, the concrete fracture highlights a roughness, a tortuosity and eventually crack bridging; it means that a reduction factor should be introduced in Poiseuille's permeability, taking into account all the presented phenomena. As a first approximation, this reduction factor is supposed constant for any crack opening [7, 10, 12]. However, based on splitting experiments, it is shown that this reduction factor is not constant, but it increases with the crack opening [8, 9]. An empirical equation (Eqn 9) identified on the gas conductivity of a high-performance concrete disc in splitting with two parameters γ (dimensionless) and β ($m^{-\gamma}$) was introduced, and their values were characterized as -1.19 and 5.625E-5 ($m^{-\gamma}$) respectively [8, 9]. The relation used in the present contribution reads:

$$\xi_{\mathrm{u}} = \frac{[u]^{-\gamma}}{\beta} \tag{9}$$

where ξ_{u} is a dimensionless reduction factor that should account for concrete fracture roughness, tortuosity and bridging. Poiseuille's permeability accounting for the presented phenomena, noted as the modified Poiseuille's law (m^2), is given by:

$$k_{\mathrm{cr}}^{\mathrm{mp}} = \xi_{\mathrm{u}} \frac{[u]^2}{12} \tag{10}$$

In this way, the evolution of the reduction factor with the crack opening is taken into account by decreasing wall and bridging effects as cracks keep on opening.

However, it should be noted that this reduction factor is derived from a splitting experiment in which a single macrocrack forms rapidly in the diametric plane of the specimen parallel to the loading. Therefore, the effects of tortuosity and bridging of the crack are rather not the most significant. In other words, they contribute less to the reduction of the flow rate in such experiment. Consequently, it seems essential to extend this reduction factor for other experimental setups in which the effects of tortuosity and bridging of the crack on the flow rate might be significant.

2.2.3. Homogenized permeability tensor. Let us consider a representative volume element (RVE) of a volume V^{e} and characteristic length l^{e}. This RVE is crossed by a crack with a normal unit direction n^e and a surface A^{e} perpendicular to the flow, that is, $A_{\mathrm{e}} = l^{\mathrm{e}} \times \left[u_{\mathrm{n^e}}^{\mathrm{e}}\right]$, where $\left[u_{\mathrm{n^e}}^{\mathrm{e}}\right]$ is the crack opening.

Let us assume that in all directions the total flow $\mathbf{Q}$ is the sum of the flow in the bulk of the material (diffuse) $\mathbf{Q}_{\mathrm{d}}$ and in the localized crack $\mathbf{Q}_{\mathrm{cr}}$.

$$\mathbf{Q} = \mathbf{Q}_{\mathrm{d}} + \mathbf{Q}_{\mathrm{cr}} \tag{11}$$

The flow in the bulk of the material is due to the initial permeability tensor $\mathbf{K}_0^{\mathrm{e}}$ of the material assumed to be isotropic. The flow in the crack is due to the anisotropic permeability. Because the same pressure gradient applied to both flows, one can directly sum up the two permeability tensors in a local axis attached to the normal of the crack ($\mathbf{n}^{\mathrm{e}}$, $\mathbf{t}_1$, $\mathbf{t}_2$) to deduce the homogenized anisotropic permeability tensor:

$$\mathbf{K}_{\mathrm{m}}^{\mathrm{e}} = \begin{bmatrix} k_0 & 0 & 0 \\ 0 & k_0 + \dfrac{\left[u_{\mathrm{n^e}}^{\mathrm{e}}\right]^{3-\gamma}}{12\, l^{\mathrm{e}}\, \beta} & 0 \\ 0 & 0 & k_0 + \dfrac{\left[u_{\mathrm{n^e}}^{\mathrm{e}}\right]^{3-\gamma}}{12\, l^{\mathrm{e}}\, \beta} \end{bmatrix}_{(\mathbf{n}^{\mathrm{e}},\, \mathbf{t}_1,\, \mathbf{t}_2)} \tag{12}$$

where k_0 is the initial permeability.

In an FE computation, the permeability tensor $\mathbf{K}_{\mathrm{m}}^{\mathrm{e}}$ is defined for each FE considered as an RVE in its local axis. It should be noted that for total flow computation, $\mathbf{K}_{\mathrm{m}}^{\mathrm{e}}$ should be expressed in the global axis

by using rotation matrices of coordinate systems. In cases where FEs with multiple Gauss points are used, the same averaged permeability tensor is applied to each. This formulation requires finding the crack path (location and orientation) as well as the calculation of the crack opening at each integration point $\left[u_{\mathrm{n}^{\mathrm{e}}}^{\mathrm{e}}\right]$ of the crack path. The numerical method to find the crack path is given in Section 2.2.4. The crack opening assessment is detailed in Section 2.2.5.

2.2.4. Crack path. Among the numerical methods that exist in the literature to find the crack path from the continuous calculation, two post-treatment methods are retained: the topological search and the global tracking algorithm. They are briefly presented in this section. More details can be found in Refs [22, 23] for the topological search and in Ref. [24] for the global tracking algorithm.

2.2.4.1. Topological search. The method to locate the crack path is based on a topological search approach. It is a step-by-step procedure with a space step a to follow the ridge of a scalar field characterizing the degradation of the material. For the continuous model considered here, the strain field Y (see Section 2.1) is considered as the representative field of cracking because it is the most robust compared to the damage field whose values are limited to 1. The idea is that from the 2D scalar field Y, the locus of the maximum values corresponds to the crack path. For 3D domains, the crack path is successively determined in several 2D parallel cuts of the domain.

Three main steps need to be defined to find the crack path: the initiation step, the current step and the ending step.

- Initiation step

The Gauss point P_0 bearing the maximum value of the post-treated field is used to initiate the searching procedure. As no search direction is initially defined, a circle centred on P_0 with a radius equal to a is used to project the field Y. The maximum value of the convoluted profile $Y(\mathbf{s}) * \varnothing(\mathbf{s}, l_{\mathrm{c}0})$, where * is the convolution product and $\mathbf{s}$ is the curvilinear coordinate along the circle, defines the point P_2 of the crack. The first point P_0 is re-evaluated to become P_1 (because its position depends on the location of Gauss points) by taking the maximum of the convoluted profile along the profile which is perpendicular to $\overrightarrow{P_2P_0}$ at P_0. Then, current steps can be performed. As two directions are defined by points P_2 and P_1, each is considered in turn.

- Current step

From a point P_{i} and a search direction $\overrightarrow{P_{\mathrm{i}-1}P_{\mathrm{i}}}$, the point $P_{\mathrm{i}+1}$ is defined as the locus of the maximum value of the convoluted profile $Y(\mathbf{s}) * \varnothing(\mathbf{s}, l_{\mathrm{c}0})$ along the line which is perpendicular to the search direction at point P_0, defined as $\overrightarrow{P_{\mathrm{i}}P_0} = a \dfrac{\overrightarrow{P_{\mathrm{i}-1}P_{\mathrm{i}}}}{\left\|\overrightarrow{P_{\mathrm{i}-1}P_{\mathrm{i}}}\right\|}$

It is worth noting that the crack path does not depend on the space discretization of the initial simulation because the crack path is found out from the convoluted field.

- Ending step

Different criteria are considered to stop the searching procedure: Point $P_{\mathrm{i}+1}$ is out of the domain boundaries, or the maximum of the convoluted profile used to identify $P_{\mathrm{i}+1}$ is smaller than $\varepsilon_{\mathrm{D}0}$ (strain at first crack in tension).

2.2.4.2. Global tracking algorithm. This method considers an equivalent conduction problem with the direction associated to the maximum principal strain identified as the direction of the flux. The compatible crack paths correspond to iso values perpendicular to the direction of the flux, that is, maximum principal strain. At the end, the iso line corresponding to the crack path is the one passing through the Gaussian point with the highest nonlocal equivalent strain. More details can be found in Ref. [24].

Compared to the topological search method (Section 2.2.4.1), this procedure is directly applicable in 3D. However, the hypothesis of pure mode I crack opening must be valid.

2.2.5. Crack opening assessment. In order to assess the crack opening, a post-treatment of the strain field obtained from the FE calculation is performed. After identifying the crack path, the crack opening is calculated by comparing the computed strain field ε_{FE} and the analytical strain profile $\varepsilon_{SD} = [u]\delta(x)$ corresponding to a strong discontinuity (displacement jump) along a line (1D profile) perpendicular to the crack path. As the analytical strain profile is a Dirac-like function, a direct comparison cannot be performed with the numerical strain profile. Thus, a convolution product is applied on both profiles by using a Gaussian function $\varnothing$. By considering the equality of both convoluted profiles at the crack location x_0 [25], one can obtain an estimation of the crack opening:

$$[u]^e = \frac{(\varepsilon_{FE} * \varnothing)(x_0)\int_l \varnothing(x - x_0)dx}{\varnothing(0)} \tag{13}$$

This method also gives an error indicator $\Delta(x_0, [u])$ along the crack path for each perpendicular profile by comparison between the numerical profile and the strong discontinuity one.

$$\Delta(x_0, [u]^e) = \frac{\int_l |(\varepsilon_{SD} * \varnothing)(x, x_0, [u]^e) - (\varepsilon_{FE} * \varnothing)(x)|dx}{\int_l (\varepsilon_{FE} * \varnothing)(x)dx} \tag{14}$$

Equation 14 gives only a model error and should be seen by the user as an indicator of the quality of the hypothesis made by comparing the FE strain profile and the strain profile of a strong discontinuity.

2.2.6. Staggered algorithm. The advantages of a post-treatment procedure for the gas transfer problem are that its implementation is not intrusive in the FE tool and that the mechanical problem can be solved by means of any constitutive models and FE code.

The algorithm of the post-treatment procedure to determine the total leakage rate can be summarized as follows (Figure 1). After solving the mechanical problem, the crack path (crack surface in 3D) is defined first (see Section 2.2.4). Secondly, the crack opening is estimated by using the analytical analogy (see Section 2.2.5), then the local permeability of the FE at its integration point in the crack surface is calculated. For the undamaged elements, the permeability is supposed to be equal to the initial one. Thirdly, the diffusion problem imposing a pressure gradient is solved (more details

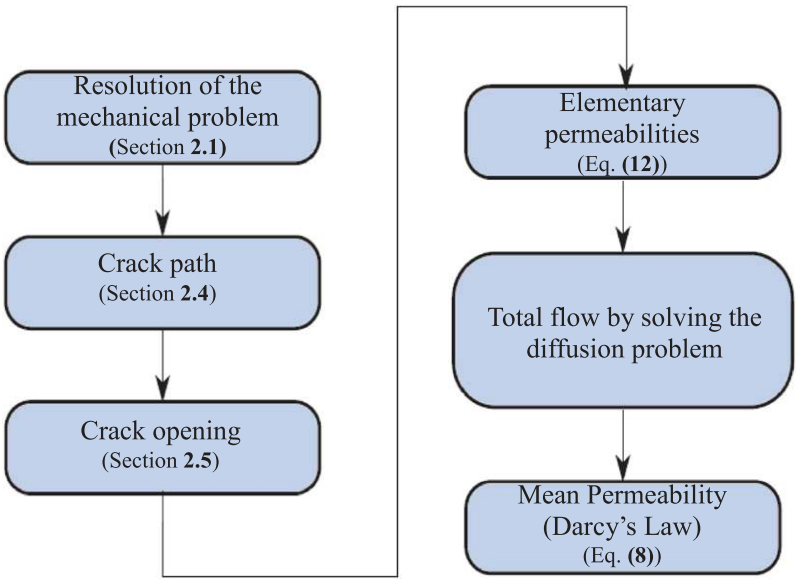

Figure 1. Algorithm, type staggered, for the mechanical state-permeability coupling.

can be found in Section 5). Finally, by means of Darcy's law, the mean structural permeability (conductivity) in the direction of the pressure gradient can be calculated out of the diffusion problem.

3. EXPERIMENTAL SETUP

The experiment consists of a Brazilian splitting test applied on dry mortar specimens (Figure 2). The samples have a cylindrical shape of 40 mm height and 110 mm diameter. It is worth noting that the samples are not perfectly cylindrical; a difference of approximately 0.1 mm in diameter is observed due to the geometry defaults of the steel mould. Although this test is rather complex to control in the post-peak regime, it presents a single macrocrack in the specimen which is an advantage for the gas transfer part of the experiment. Furthermore, the crack position is known a priori. Thus, it can be instrumented for the test control and accurately measured by DIC. In the experiments, the test is controlled by means of the relative displacement between two points on the face (S_b) with the largest diameter. Those points are located at a distance of 10 mm from the centre of the disc. This relative displacement is identical to the COD for large values. The smallest face (S_s) is discretized by means of a speckle pattern (Figure 3a) to perform a DIC analysis and to obtain the 2D horizontal displacement field on the face. A window of interest is placed around the crack as shown in Figure 3b to estimate the crack opening, that is, the jump in the horizontal displacement field along the crack path.

In the post-peak regime, dry nitrogen flow rate measurements are taken after partially unloading the sample to avoid rupture due to the coupling between creep and damage (Figure 4).

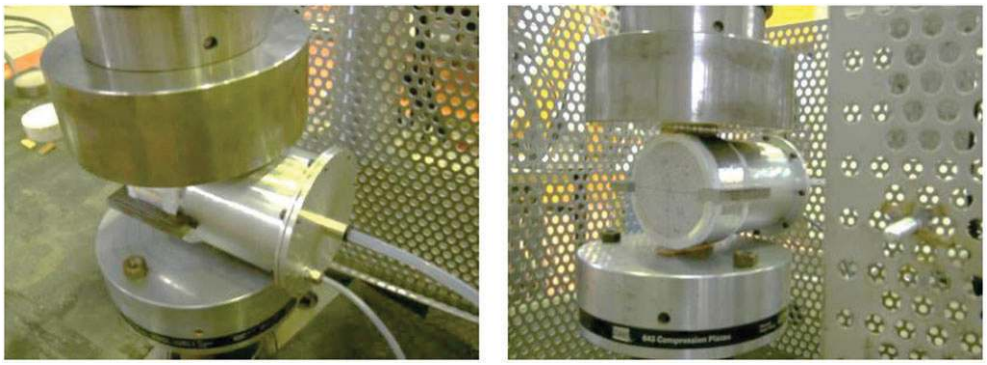

Figure 2. Conductivity analysis whilst performing a Brazilian test on a mortar sample.

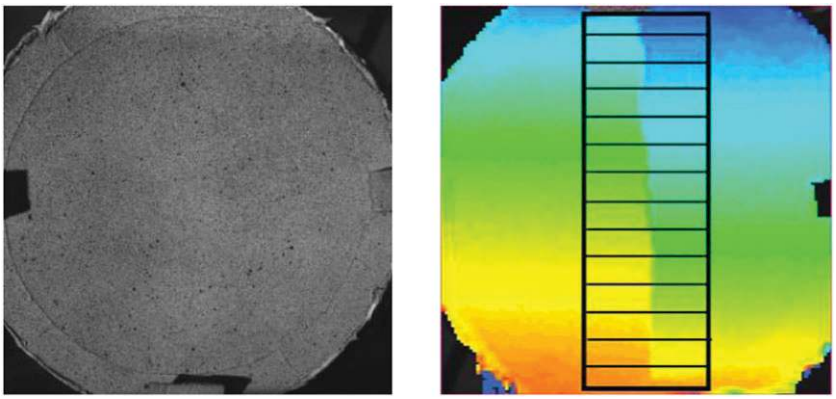

(a) (b)

Figure 3. Speckle pattern (a) and the horizontal displacement field at failure of the specimen face with the grid to estimate the crack opening displacement along the crack path (b).

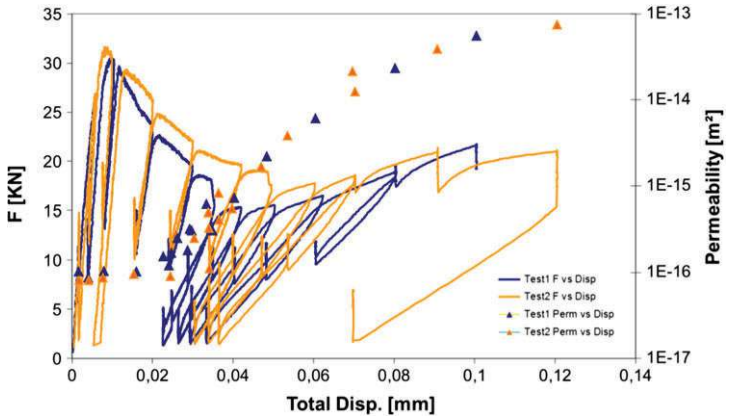

Figure 4. Mechanical behaviour and permeability evolution versus the total displacement for two mortar specimens.

3.1. Mechanical and gas transfer behaviour

The mechanical response (applied force vs the relative horizontal displacement) and the mean permeability evolution of two mortar specimens are shown in Figure 4, with a good repeatability. Classically, the mechanical response starts with an elastic part, reaches a peak, and the softening behaviour ends up by a complete split of the specimen. At horizontal displacement equal to approximately 0.034 mm, the specimen is split and the behaviour afterwards is described by the two half portions of the specimen subjected to compression which explains why the bearing capacity is increasing again. A detailed analysis comparing the COD measures obtained with the sensor and with the DIC has shown that there is a 3D effect on the specimen behaviour. In particular, the 3D effect is important between the peak (start of the macrocrack propagation) and the complete splitting of the specimen obtained for a relative displacement of approximately 0.034 mm. Indeed, as also described in Refs [9, 10, 12], the crack initiates on the largest face (S_b) and then propagates in the longitudinal direction to the other face (S_s).

The mean permeability evolution can be described by the three regimes proposed in Ref. [1]. For displacements varying from 0 to 0.03 mm, a slight increase in the mean permeability is observed. Afterwards, a large increase in the mean permeability begins where both crack opening and connectivity are increasing. Finally, the increase rate of the mean permeability is slower because the connectivity is already established.

4. COMPARISON WITH EXPERIMENTS

This numerical application is a simulation of one of the two physical experiments presented in Section 3 to validate the mechanical model, the crack property assessment and the coupling with transfer properties. The steel bearing plates are modelled as elastic plates with high Young's modulus ($E = 300$ GPa) and the Poisson's ratio of mortar ($\nu = 0.2$) in order to avoid a local confinement effect of mortar. Numerical simulations are performed in the FE code CAST3M [32] with 20 807 four-node tetrahedral elements. Due to the two symmetries of the problem, the computational domain is reduced to a quarter of the specimen. Thus, the relative displacement which controls the test is now reduced to the total displacement at point P. The mesh (Figure 5b) is generated with the same conicity than the real specimen in order to reproduce the 3D effect in the simulations. An arc-length procedure driven by the maximum strain is performed to solve the mechanical problem in the post-peak regime [33, 34].

4.1. Mechanical description of the splitting test

A calibration of the mechanical model parameters is performed by considering a trial-and-error process applied on the physical response. The parameter set of the SBNL Mazars model is given in Table I.

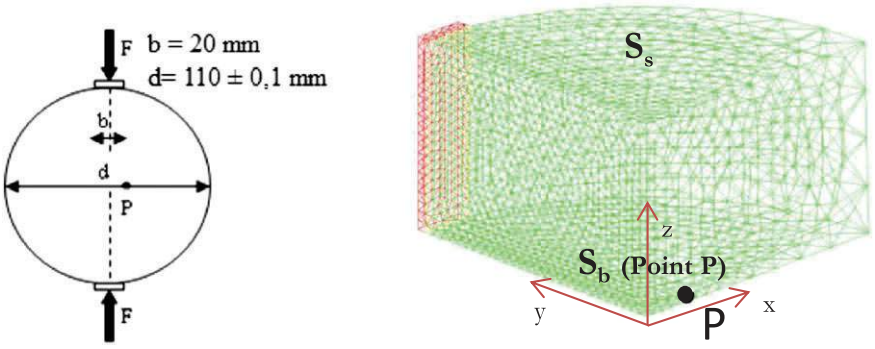

(a) (b)

Figure 5. Brazilian splitting test (a) face S_b (b) 3D conic finite element mesh.

Table I. Set of parameters.

Parameter	SBNL
Y_{D0}	3.5×10^{-4}
A_c	1.4
A_t	0.88
B_c	800
B_t	4050
β_s	1.06
l_{c0}	7.5 mm
E	18 MPa
ν	0.2
γ	−1.19
β	5.625E-5
μ	1.79×10^{-5} Pa s

The comparison between the numerical model and the experiment made on the mechanical response (force vs displacement at P) is shown in Figure 6. This result shows that the SBNL damage model provides a good estimation of the physical response in describing the behaviour even after the total split. This is possible because both the damage and the strain are well localized at failure without spurious diffusion as for other nonlocal approaches. One can see that the Mazars model presents an exaggerated snapback (elastic discharge of the face S_b), where the displacement of point P decreases from about 0.035 to 0.0305 mm. Indeed, this model does not account for the permanent deformation, and consequently, the elastic discharge described by the model is more important.

4.2. Damage propagation

Damage fields at four loading levels given by the SBNL model are presented in Figure 7. At peak A, damage is initiated in the centre of the surface S_b. In the post-peak behaviour (between A and B), damage propagates on the surface S_b and in the longitudinal direction towards the surface S_s. At point B, the damage starts to occur on the surface S_s, then it propagates on this face from the centre towards the bearing plates. It provides a rotation of the specimen with respect to the vertical axis, yielding a decrease of the displacement at point P. The latter ends up by a total split (point C) and the end of the snapback phenomenon. The behaviour becomes the one of the half portion, and almost all the crack surface is totally damaged. D corresponds to the last state, with displacement of point P equal to approximately 0.1 mm. At some points (three), a mechanical discharge is performed to compare the structural stiffness with the experimental one.

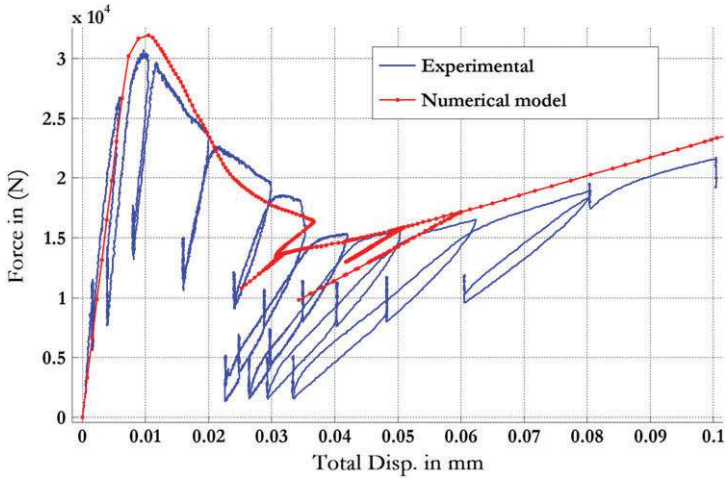

Figure 6. Mechanical response (force vs total horizontal displacement of point P) described by stress-based nonlocal damage model compared with experimental response.

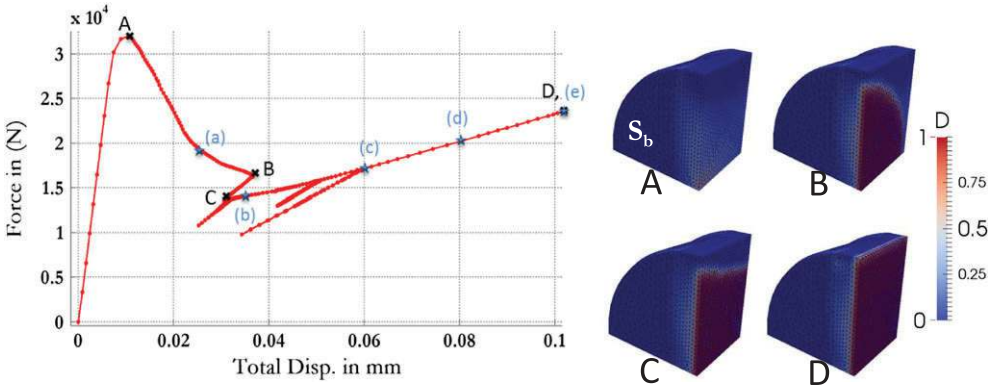

Figure 7. Damage fields given by stress-based nonlocal damage model at four loading levels (A), (B), (C) and (D).

In this specific example, the crack path is obviously the symmetry surface parallel to the loading, and there is no need to perform one of the two procedures presented in Section 2.2.4. However, they have been checked to provide the right solution.

4.3. Crack opening displacements

The method presented in Section 2.2.5 is applied on the splitting simulation to determine numerically the CODs.

A comparison is made between CODs obtained experimentally by the DIC technique and numerically by analogy, with the strong discontinuity method at five different loadings that correspond respectively to horizontal displacements at point P: (a) 0.0247 mm, (b) 0.033 mm, (c) 0.06 mm, (d) 0.08 mm and (e) 0.1 mm (Figures 7–9).

On the face S_s, at state (a), the analytical method fails to assess properly the COD (Figure 8). Indeed, the assumption for this method is to have a strong discontinuity. Because the cracking is not fully developed on the face S_s (rear face), the assumption is not fulfilled, and consequently, the method cannot reproduce properly the COD on that face. Moreover, the error indicator for the analytical method (Eqn 14) shows a very high relative error (>60%; Figure 10). This error indicator is indeed very useful to decide whether the crack opening estimation based on the FE computation can be

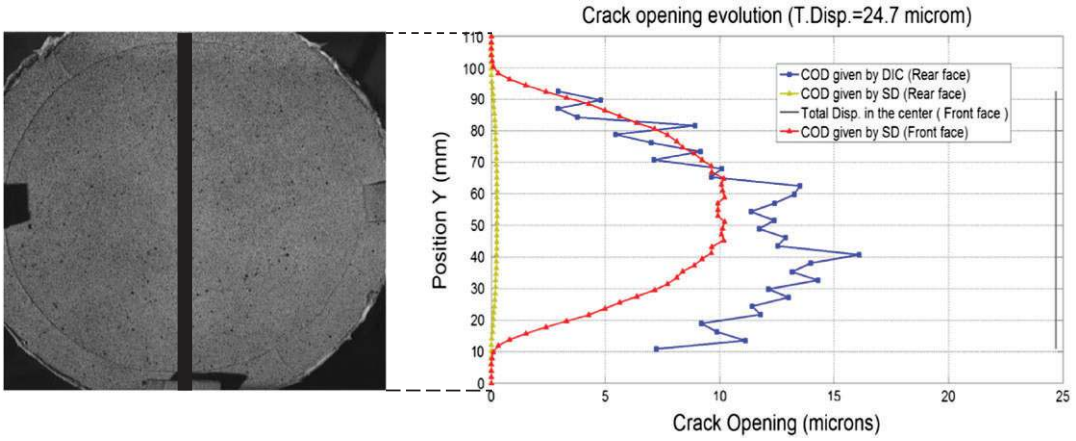

(a)

Figure 8. Crack opening profile along the crack path at (a) 0.0247 mm.

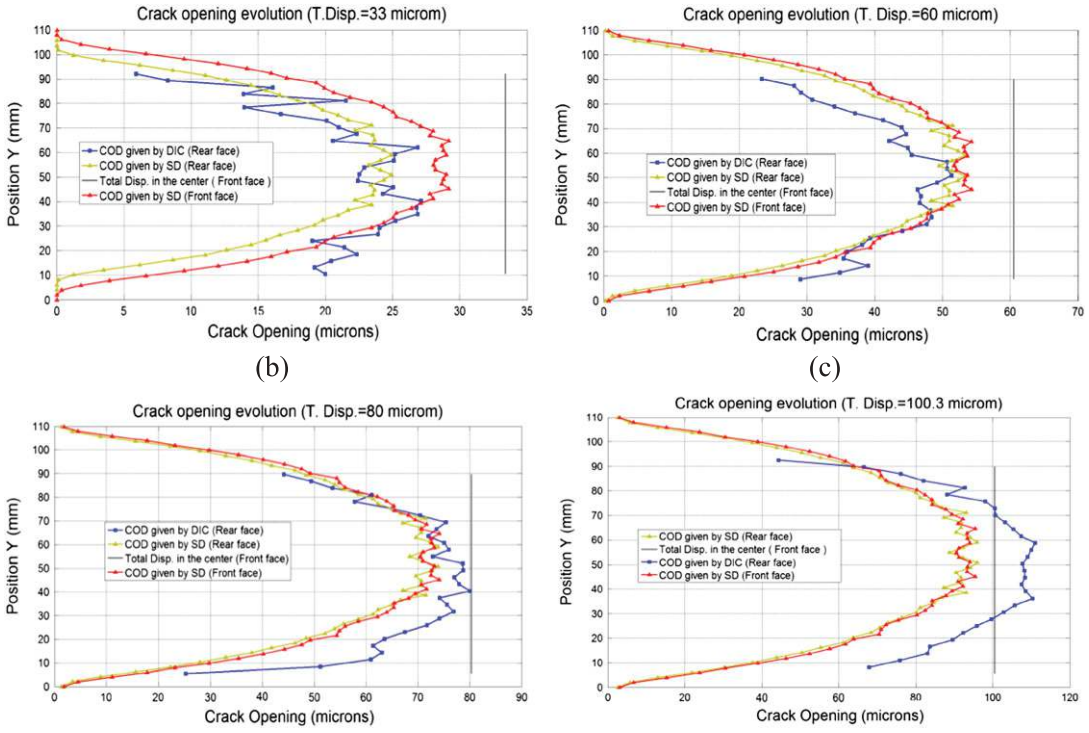

(b) (c) (d) (e)

Figure 9. Crack opening profiles for four loading states corresponding to total horizontal displacement of P equal to (b) 0.033 mm, (c) 0.06 mm, (d) 0.08 mm and (e) 0.1 mm.

used if the experimental results are not known. Nevertheless, on the face S_b (front face) where the cracking is developed, the calculated COD given by the analytical approach is in the same order as the one provided by DIC, and the error indicator shows a relative error of around 20% in the central part (zone of interest where the cracking is dominant).

The points (b), (c), (d) and (e) are located after the split at 0.033, 0.06, 0.08 and 0.1 mm respectively (Figure 7). It is shown that after the split (point C), the cracking is developed on both faces. Moreover, at those states, the numerically assessed CODs are in great agreement with the DIC results (Figure 9).

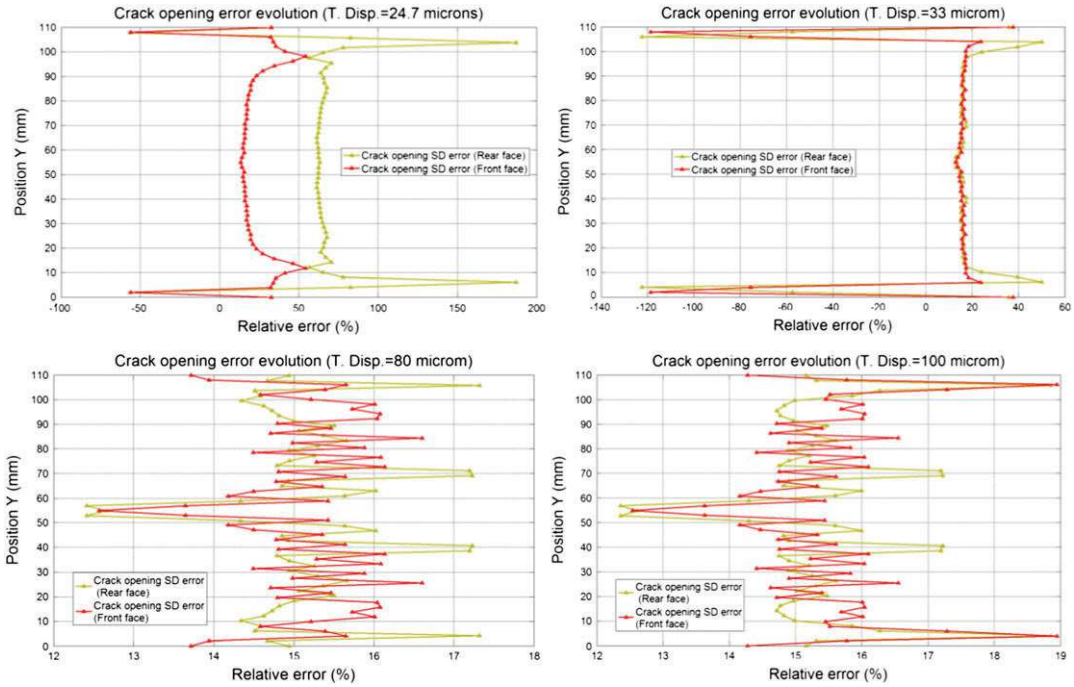

Figure 10. Relative error on crack opening profiles for four loading states corresponding to total horizontal displacement of P equal to (a) 0.0247 mm, (b) 0.033 mm, (d) 0.08 mm and (e) 0.1 mm.

This shows again that once the crack is fully developed, the herein proposed method is well positioned to assess the crack opening. At states (b), (d) and (e), the error indicator shows a maximum error in the central part that is lower than 20% and a minimum error (13%) at mid-height where the COD is the largest (Figure 10). This shows that the system dynamics assumption is adequate and acceptable when the crack is fully developed.

4.4. Coupling permeability-mechanical state

Once the numerical description of the mechanical response for the splitting test is achieved, the algorithm presented in Section 2.2.6 (Figure 1) is applied to numerically compute the total flow rate through the cracked specimen.

The next step, after assessing the crack openings along the crack path, is to compute the mean permeability tensor by using Eqn 12 (Figure 11). For the 3D splitting test, the mean permeability tensor $\mathbf{K}_{\mathrm{m}}^{\mathrm{e}}$ is given in Eqn 16. This tensor is calculated for each FE in its local frame, whereas $\mathbf{n}^{\mathrm{e}}$ is the unit vector that corresponds to the normal direction to the crack path at the FE. For this particular case of splitting test, the unit vector $\mathbf{n}^{\mathrm{e}}$ is along the axis X. The permeability tensor $\mathbf{K}_{\mathrm{m}}^{\mathrm{e}}$ is directly expressed in the global axis. The total flow rate can be computed by solving a diffusion problem in the volume by applying a pressure gradient between the two faces S_b and S_s (Figure 11).

$$\mathbf{K}_{\mathrm{m}}^{\mathrm{e}} = \begin{bmatrix} k_0 & 0 & 0 \\ 0 & k_0 + \dfrac{\left[u_{\mathrm{X}}^{\mathrm{e}}\right]^{3-\gamma}}{12\, l^{\mathrm{e}}\, \beta} & 0 \\ 0 & 0 & k_0 + \dfrac{\left[u_{\mathrm{X}}^{\mathrm{e}}\right]^{3-\gamma}}{12\, l^{\mathrm{e}}\, \beta} \end{bmatrix}_{(\mathbf{X},\,\mathbf{Y},\,\mathbf{Z})} \tag{16}$$

The diffusion problem is solved by introducing all matrices $\mathbf{K}_{\mathrm{m}}^{\mathrm{e}}$ in the FE software (CAST3M [33]) and imposing the pressure boundary conditions shown in Figure 11. Eventually, the mean structural permeability (gas conductivity) is calculated by applying Darcy's law (Eqn 8).

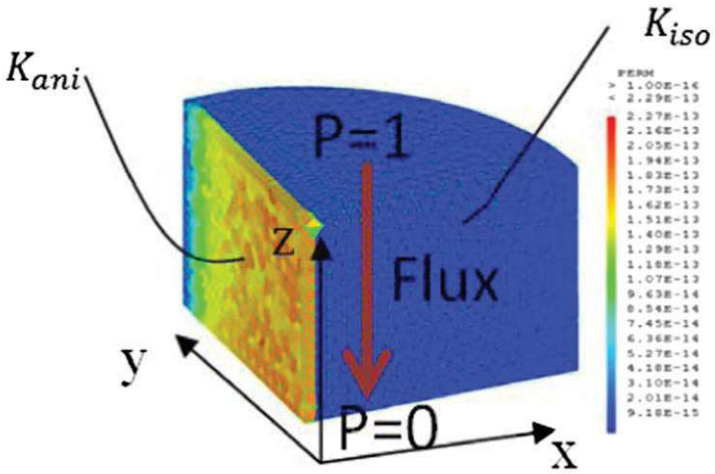

Figure 11. Solving the diffusion problem by applying a pressure gradient.

The evolution of the mean structural permeability calculated from the experiment versus the estimated one as a function of the horizontal displacement at point P is presented in Figure 12. Two cases are considered. In the first case, the concrete crack surfaces are supposed to be perfectly smooth and straight according to Poiseuille's hypothesis ($\xi = 1$). In the second case, the empirical relation for the correction factor proposed in Refs [8, 9] is considered (Eqn 9). In the phase where the crack is opened, the nonmodified Poiseuille's model overestimates the mean structural permeability (flow through the cracked structure) with respect to the experimental results, whilst the proposed model that includes the parameters proposed in Refs [8, 9] shows a good agreement with respect to experimental results. This shows that those parameters are also valid for OC when a macrocrack is developed. Moreover, less agreement between the proposed model and the experimental measurements is seen in the transition phase from microcracking to macrocracking. In this phase, the quality of the crack opening assessment is lower, and consequently, dispersion in the mean structural permeability estimation is seen.

Furthermore, despite that the study in Ref. [9] is on water conductivity of concrete, the results found in the latter study are in a good agreement (Figure 12) with the results of the study presented in this paper (gas conductivity of mortar), especially at total displacement equal to 0.1 mm. This means that the mean structural permeability is governed by the crack opening, and that this permeability tends to be independent of the percolated fluid when the crack opening is very large.

The mesh dependency analysis is illustrated in Figure 13. For computational time reason, only two meshes of mean element sizes of 3.3 and 2 mm were addressed. Based on Figure 13b, it is clear that

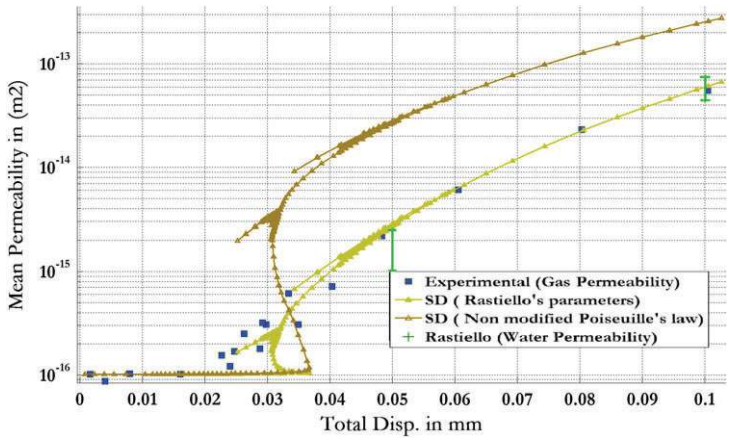

Figure 12. Estimated mean permeability evolution versus total displacement of point P.

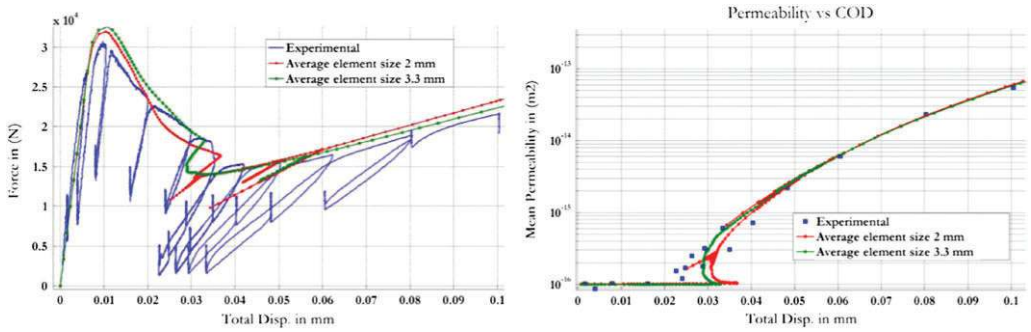

(a) (b)

Figure 13. Mesh sensitivity on mechanical global results (a) and mean permeability (b).

there is no mesh dependency once the crack is fully formed and widely opened. The reason is that by using the SBNL approach, as stated in Ref. [20], the strain is fully localized in a band with a width of one element. Thus, the maximum strain is mesh dependent and inversely proportional to the mesh size. In contrary, the crack opening, that is, a displacement quantity, which is roughly the product of the strain perpendicular to the crack path, is mesh independent and thus the transfer properties.

In addition, for intermediate states, a slight mesh dependency is observed in the mean permeability evolution. This is completely related to the mechanical response for which the snapback initiation is not exactly for the same mechanical state (Figure 13a). This is highlighted in the transfer property response due to the great evolution upon the crack propagation. Snapback is not that easy to capture and follow in a quasi-static manner. Even with a nonlocal approach, slight differences are observed. One may also suspect that the complete mesh independency could be reached only with smaller mesh sizes.

5. CONCLUSIONS

This contribution presents an original gas transfer modelling as a post-treatment procedure based on a mechanical model for concrete structures undergoing mode I cracking. A semi-discrete approach in a continuous framework is proposed to find a numerical coupling between structural permeability and mechanical properties for concrete/mortar. For validation purposes, an original experimental campaign on gas conductivity measurement during a splitting test is presented. Due to a 3D effect, the crack crosses the specimen well after the peak force. Until this point, the leakage rate does not change much because the connectivity between the two faces is not yet fully established. Upon the crossing of the crack, the leakage rate increases by much due to the development of cracks and connectivity. Once the splitting is complete, the bearing capacity starts increasing and the leakage rate increase is reduced because it is only due to the opening of the main crack.

After calibration of material model parameters on the global mechanical response, the SBNL damage model describes accurately the global behaviour of the specimen subjected to the splitting test presented here. The model is able to reproduce the global behaviour even after the split of the specimen. Damage initiation and propagation are similar to experimental observation. In the crack surface, COD is assessed by using an analytical method based on the analogy with the strong discontinuity approach. When a macrocrack is formed, the results given by the latter method show a good agreement with experimental measurements. Thus, the proposed mechanical model is able not only to reproduce the global response but also to provide good estimation of local quantities.

It was shown that in the phase where there is an opened crack, the nonmodified Poiseuille's model of perfectly smooth parallel plates overestimates the mean structural permeability (flow rate through the cracked structure) with respect to the experimental results, whilst the proposed model that includes the parameters found in Refs [8, 9] shows a good agreement with respect to experimental results. This shows that those parameters are also valid for OC when a macrocrack is developed.

Moreover, less agreement between the proposed model and the experimental measurements is seen in the transition phase from microcracking to macrocracking. In this phase, the quality of the crack opening estimation is lower, and consequently, dispersion in the mean structural permeability estimation is seen. A comparison has been made between the calculated mean structural permeability in this study (gas conductivity of mortar) and the one calculated in the study on water permeability of concrete [8, 9]. The results found in the latter study are in a good agreement with the results of the study presented in this paper (gas conductivity of mortar), especially at high level of cracking. This means that the mean structural permeability is governed by the crack opening, and that this permeability tends to be independent of the percolated fluid when the crack opening is very large. Finally, the proposed model is based on a staggered algorithm which is simple and easy to implement. One can solve first the mechanical problem and then solve the gas transfer one. This model is validated by two different studies that emphasize again that the description of the crack opening field is the key issue for the estimation of the mean structural permeability. Finally, mesh-independent results are obtained with the proposed model. Consequently, if the mechanical problem is well modelled, then the gas transfer problem, based on local mechanical quantities, is well modelled as well. It should be noted, however, that this proposition is limited to mode I cracking and definitely not valid when shearing occurs. The perspective of this work is to extend the proposed model to other cracking modes. Moreover, it seems essential to extend the reduction factor in the modified Poiseuille's permeability to general cases in which all phenomena that contribute to the flow rate reduction occur.

ACKNOWLEDGEMENTS

The authors gratefully acknowledge the funding support from France's National Research Agency through the 'MACENA' project (ANR-11-RSNR-012).
3SR is part of the LabEx Tec 21 (Investissements d'Avenir grant agreement no. ANR-11-LABX-0030).

REFERENCES

1. Choinska M, Khelidj A, Chatzigeorgiou G, Pijaudier-Cabot G. Effects and interactions of temperature and stress-level related damage on permeability of concrete. *Cement and Concrete Research* 2007; **37**(1):79–88. doi:10.1016/j.cemconres.2006.09.015.
2. Chatzigeorgiou G, Vincent P, Abdelhafid K, Pijaudier-Cabot G. Coupling between progressive damage and permeability of concrete: analysis with a discrete model. *International Journal for Numerical and Analytical Methods in Geomechanics* 2005; **29**(10):1005–18. doi:10.1002/nag.445.
3. Picandet V, Khelidj A, Bastian G. Effect of axial compressive damage on gas permeability of ordinary and high-performance concrete. *Cement and Concrete Research* 2001; **31**(11):1525–32. doi:10.1016/S0008-8846(01)00546-4.
4. Gérard B. Contribution des couplages mécanique-chimie-transfert dans la tenue à long terme des ouvrages de stockage de déchets radioactifs. PhD Thesis, ENS Cachan 1996.
5. Gerard B, Breysse D, Ammouche A, Houdusse O, Didry O. Cracking and permeability of concrete under tension. *Materials and Structures* 1996; **29**(187):141–51.
6. Dal Pont S, Schrefler BA, Ehrlacher A. Experimental and finite element analysis of a hollow cylinder submitted to high temperatures. *Materials and Structures* 2005; **38**(281):681–90. doi:10.1617/14167.
7. Picandet V, Khelidj A, Hervé B. Crack effects on gas and water permeability of concretes. *Cement and Concrete Research* 2009; **39**(6):537–47. doi:10.1016/j.cemconres.2009.03.009.
8. Rastiello G. Influence de la fissuration sur le transfert de fluides dans les structures en béton. Stratégies de modélisation probabiliste et étude expérimentale. PhD Thesis, IFSTTAR, 2013.
9. Rastiello G, Boulay C, Dal Pont S, Tailhan JL, Rossi P. Real-time water permeability evolution of a localized crack in concrete under loading. *Cement and Concrete Research* 2014; **56**:20–28. doi:10.1016/j.cemconres.2013.09.010.
10. Wang K, Daniel J, Surendra S, Alan K. Permeability study of cracked concrete. *Cement and Concrete Research* 1997; **27**(3):381–93. doi:10.1016/S0008-8846(97)00031-8.
11. Akhavan A, Seyed-Mohammad-Hadi S, Farshad R. Quantifying the effects of crack width, tortuosity, and roughness on water permeability of cracked mortars. *Cement and Concrete Research* 2012; **42**(2):313–20. doi:10.1016/j.cemconres.2011.10.002.
12. Aldea CM, Shah SP, Karr A. Permeability of cracked concrete. *Materials and Structures* 1999; **32**(219):370–76. doi:10.1007/BF02479629.
13. Moes N, Dolbow J, Belytschko T. A finite element method for crack growth without remeshing. *International Journal for Numerical Methods in Engineering* 1999; **46**(1):131–150.
14. Strouboulis T, Babuška I, Copps K. The design and analysis of the generalized finite element method. *Computer Methods in Applied Mechanics and Engineering* 2000; **181**(1-3):43–69. doi:10.1016/S0045-7825(99)00072-9.

15. Oliver J, Huespe AE, Sánchez PJ. A comparative study on finite elements for capturing strong discontinuities: E-FEM vs X-FEM. *Computer Methods in Applied Mechanics and Engineering* 2006 John H. Argyris Memorial Issue. Part I,; **195**(37–40):4732–52. doi:10.1016/j.cma.2005.09.020.
16. Jourdain X, Colliat J-B, De Sa C, Benboudjema F, Gatuingt F. Upscaling permeability for fractured concrete: meso–macro numerical approach coupled to strong discontinuities. *International Journal for Numerical and Analytical Methods in Geomechanics* 2014; **38**(5):536–50. doi:10.1002/nag.2223.
17. Bolander JE, Saito S. Fracture analyses using spring networks with random geometry. *Engineering Fracture Mechanics* 1998; **61**(5–6):569–591. doi:10.1016/S0013-7944(98)00069-1.
18. Cusatis G, Bažant Z, Cedolin L. Confinement-shear lattice model for concrete damage in tension and compression: II. computation and validation. *Journal of Engineering Mechanics* 2003; **129**(12):1449–1458. doi:10.1061/(ASCE) 0733-9399.
19. Mazars J. Application de la mécanique de l'endommagement au comportement non linéaire et à la rupture de béton de structure. PhD Thesis, Université Pierre et Marie Curie, 1984.
20. Giry C, Dufour F, Mazars J. Stress-based nonlocal damage model. *International Journal of Solids and Structures* 2011; **48**(25–26):3431–3443. doi:10.1016/j.ijsolstr.2011.08.012.
21. Pijaudier-Cabot G, Bazant ZP. Nonlocal damage theory. *Journal of Engineering Mechanics* 1987; **113** (10):1512–1533.
22. Giry C, Oliver-Leblond C, Dufour F, Ragueneau F. Cracking analysis of reinforced concrete structures. *European Journal of Environmental and Civil Engineering* 2014; **18**(7):724–37. doi:10.1008/19648189.2014.881756.
23. Bottoni M, Dufour F, Giry C. Topological search of the crack pattern from a continuum mechanical computation. *Engineering Structures* 2015; **99**:346–359. doi:10.1016/j.engstruct.2015.05.005.
24. Dufour F, Legrain G, Pijaudier-Cabot G, Huerta A. Estimate of crack opening from a 2D continuum-based FE computation. *International Journal for Numerical and Analytical Methods in Geomechanics* 2012; **36**(16):1813–1830. doi:10.1002/nag.1097.
25. Dufour F, Pijaudier-Cabot G, Choinska M, Huerta A. Extraction of a crack opening from a continuous approach using regularized damage models. *Computers and Concrete* 2008; **5**(4):375–388.
26. Pijaudier-Cabot G, Dufour F, Choinska M. Permeability due to the increase of damage in concrete: from diffuse to localized damage distributions. *Journal of Engineering Mechanics* 2009; **135**(9):1022–1028. doi:10.1061/(ASCE) EM.1943-7889.0000016.
27. Simone A, Askes H, Sluys LJ. Incorrect initiation and propagation of failure in non-local and gradient-enhanced media. *International Journal of Solids and Structures* 2004; **41**(2):351–363. doi:10.1016/j.ijsolstr.2003.09.020.
28. Darcy H. Les Fontaines Publiques de la Ville de Dijon. Dalmont, Paris. 647 p. & atlas, 1856.
29. Snow DT. A parallel plate model of permeable fractured media. PhD Thesis, University of California Berkley, 1969.
30. De Marsily G. *Quantitative hydrogeology: Groundwater Hydrology for Engineers*. Michigan University, Academic Press, 1986.
31. Zimmerman R, Bodvarsson G. Hydraulic conductivity of rock fractures. *Transport in Porous Media* 1996; **23**:1–30.
32. Cast3m, Finite element software developed by CEA, France. Accessed on February 2013. http://www-cast3m.cea.fr/ .
33. Rodríguez-Ferran A, Huerta A. Error estimation and adaptivity for nonlocal damage models. *International Journal of Solids and Structures* 2000; **37**(48–50):7501–7528. doi:10.1016/S0020-7683(00)00209-2.
34. Pegon P, Anthoine A. Numerical strategies for solving continuum damage problems with softening: application to the homogenization of masonry. *Computers & Structures* 1997; **64**(1–4):623–642. doi:10.1016/S0045-7949(96) 00153-8.